AD-A118 269 NAVAL POSTGRADUATE SCHOOL MONTEREY CA F/G 20/4
AN EXPERIMENTAL TECHNIQUE FOR THE STUDY OF VELOCITY PROFILES IN--ETC(U)
MAR 82 A F PELLIN

UNCLASSIFIED NL

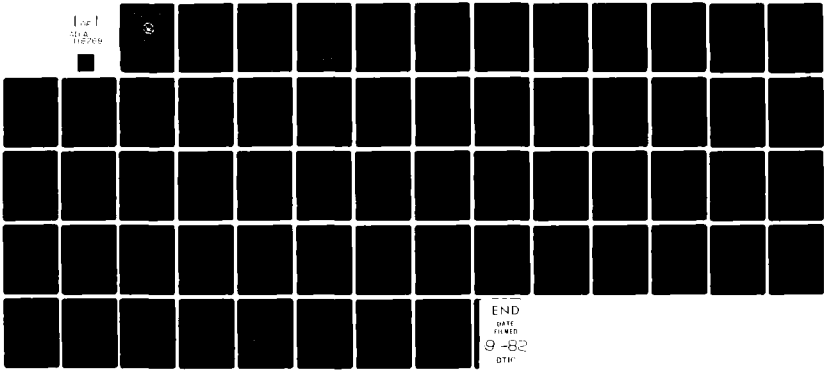

NAVAL POSTGRADUATE SCHOOL
Monterey, California

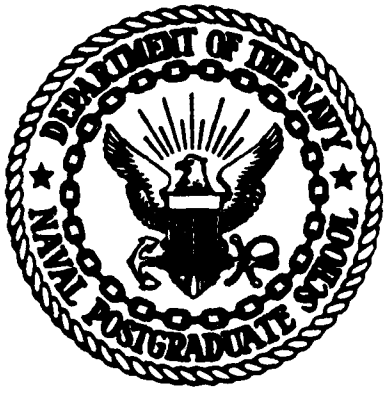

THESIS

AN EXPERIMENTAL TECHNIQUE FOR THE STUDY OF VELOCITY PROFILES IN A GROWING DROPLET USING A PULSED NITROGEN LASER

by

August Frederick Pellin III

March 1982

Thesis Advisor: W. G. Culbreth

Approved for public release; distribution unlimited.

SECURITY CLASSIFICATION OF THIS PAGE (When Data Entered)

REPORT DOCUMENTATION PAGE		READ INSTRUCTIONS BEFORE COMPLETING FORM
1. REPORT NUMBER	2. GOVT ACCESSION NO. AD-A118269	3. RECIPIENT'S CATALOG NUMBER
4. TITLE (and Subtitle) An Experimental Technique for the Study of Velocity Profiles in a Growing Droplet Using a Pulsed Nitrogen Laser		5. TYPE OF REPORT & PERIOD COVERED Master's Thesis; March 1982
		6. PERFORMING ORG. REPORT NUMBER
7. AUTHOR(s) August Frederick Pellin III		8. CONTRACT OR GRANT NUMBER(s)
9. PERFORMING ORGANIZATION NAME AND ADDRESS Naval Postgraduate School Monterey, California 93940		10. PROGRAM ELEMENT, PROJECT, TASK AREA & WORK UNIT NUMBERS
11. CONTROLLING OFFICE NAME AND ADDRESS Naval Postgraduate School Monterey, California 93940		12. REPORT DATE March 1982
		13. NUMBER OF PAGES 61
14. MONITORING AGENCY NAME & ADDRESS(if different from Controlling Office)		15. SECURITY CLASS. (of this report) Unclassified
		15a. DECLASSIFICATION/DOWNGRADING SCHEDULE

16. DISTRIBUTION STATEMENT (of this Report)

Approved for public release; distribution unlimited.

17. DISTRIBUTION STATEMENT (of the abstract entered in Block 20, if different from Report)

18. SUPPLEMENTARY NOTES

19. KEY WORDS (Continue on reverse side if necessary and identify by block number)

Laser Velocimetry, Fluid Velocity Profiles, Flow Visualization Techniques

NAPS Number

20. ABSTRACT (Continue on reverse side if necessary and identify by block number)

An ultraviolet beam (337.1 nm) from a pulsed nitrogen gas laser fired through a fluid containing a photochromic dye produces opaque traces in the fluid along the path of the laser beam. Subsequent movement of the fluid deforms

DD FORM 1 JAN 73 1473 EDITION OF 1 NOV 65 IS OBSOLETE
S/N 0102-014-6601

SECURITY CLASSIFICATION OF THIS PAGE (When Data Entered)

the opaque traces and produces a record of the fluid flow. A high powered laser has been designed, built, and tested. Velocity distributions have been obtained in slowly forming droplets of solvent in an immiscible ambient fluid.

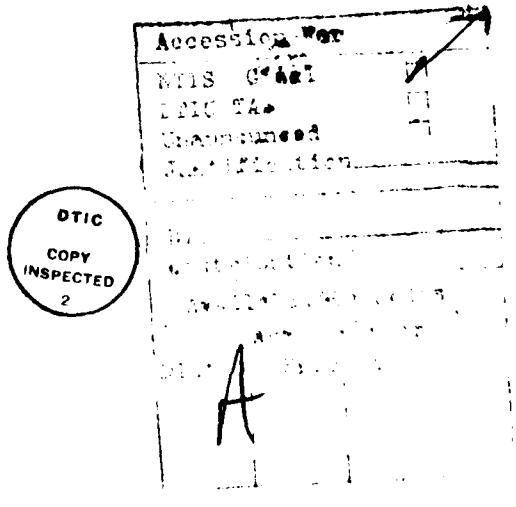

Approved for public release; distribution unlimited.

An Experimental Technique for the Study of Velocity Profiles in a Growing Droplet Using a Pulsed Nitrogen Laser

by

August Frederick Pellin III
Lieutenant, United States Navy
B.S.S.A., Miami(OHIO) University, 1976

Submitted in partial fulfillment of the requirements for the degree of

MASTER OF SCIENCE IN MECHANICAL ENGINEERING

from the

NAVAL POSTGRADUATE SCHOOL
March, 1982

Author: _____

Approved by: _____
Thesis Advisor

_____
Second Reader

_____
Chairman, Department of Mechanical Engineering

_____
Dean of Science and Engineering

ABSTRACT

An ultraviolet beam (337.1 nm) from a pulsed nitrogen gas laser fired through a fluid containing a photochromic dye produces opaque traces in the fluid along the path of the laser beam. Subsequent movement of the fluid deforms the opaque traces and produces a record of the fluid flow. A high powered laser has been designed, built, and tested. Velocity distributions have been obtained in slowly forming droplets of solvent in an immiscible ambient fluid.

TABLE OF CONTENTS

LIST OF TABLES

LIST OF FIGURES

I. INTRODUCTION

Valuable insight into the hydrodynamics of fluid flow can be obtained by "seeding" the flow with some tracer material and by analyzing the subsequent movement of the tracer. Aluminum flakes have been used to demonstrate surface flows in liquids [1]. Food dyes are often used in water and smoke streaks can provide histories of air flow. These flow visualization techniques provide excellent quantitative measurements of fluid flow phenomenon, and, through the use of photography, qualitative measurements of flow field velocity distribution can be obtained. In cases where solid particles are used as tracer materials, errors can result when tracer particles do not accurately follow the flow streamlines.

In the present work, the use of a relatively new flow visualization and measurement technique is described. The tracer chosen was a photochromic pyrospiran dye that, while dissolved in a hydrocarbon solvent, changed in color from transparent to deep violet when exposed to ultraviolet light. A pulsed nitrogen gas laser directed at a fluid containing the dye was repeatedly fired into the fluid producing violet traces along the path of the laser beam. Subsequent motion of the fluid deformed the traces and produced a time history of the hydrodynamics.

Analysis of the data included photographing the flow, digitizing the position of the traces, correcting for optical refraction, and computing the local flow velocities.

A high powered laser was constructed based on a Blumenthal circuit [2] producing ultraviolet light at a wavelength of 3371 Angstroms. The internal flow of dispersed droplets of a hydrocarbon solvent growing in an immiscible ambient fluid was analyzed to verify the use of the technique.

II. PREVIOUS WORK

Flow visualization through the use of photochromic dye was first introduced by Popovich and Hummel in 1966 [3]. They found that by dissolving 0.1% by weight of 2(2,4-dinitro benzyl)-pyridine (DNBP) in 95% ethanol, blue tracer lines would result in the initially clear fluid when exposed to the focused beam from a high intensity xenon flash tube. Quartz plates were used in the test section to minimize the absorption of the ultraviolet light from the flash tube. The pyridine dye shifted in color from transparent to violet within 3 microseconds and, if not reexposed, reverted back to its transparent state within several milliseconds. The technique was used to look at the viscous sublayer in turbulent pipe flow. The non-invasiveness of the technique was noted.

The production of DNBP and its optical characteristics are explained in references [4] and [5]. It changes color when exposed to light in the relatively wide range of ultraviolet to 4000 Angstroms.

Popovich and Hummel [6] employed their "flash photolysis" technique using pyridine dye in ethanol flowing through a smooth-walled rectangular aluminum duct. Photographs were taken of 1 mm long traces produced in the ethanol by a xenon flash tube 1.4 milliseconds after the

creation of the trace. The deformation of the traces were analyzed to yield the velocities in the laminar sublayer and in the buffer layer. It was noted that measurements beyond Y+ = 17, where

$$Y+ = Y \sqrt{T/\rho}/v \qquad (1)$$

were not always possible. Results were compared with Reichardt's and Diesler's velocity curves and showed good agreement.

Due to the toxicity of DNBP, the use of 1,3,3-trimethylindoline-6'-nitro-benzospiropyran (TNBSP) was preferable. This dye also dissolved easily in organic solvents and responded to ultraviolet light in approximately the same manner as DNBP after ultraviolet irradiation. TNBSP transformed from a transparent state to a violet color (5250 Angstroms) and reverted back again in a matter of seconds. Production and characteristics of TNBSP are explained by Berman, et al [7].

Humphrey, et al [8] documented the fact that high fluxes of energy from an ultraviolet light source can drastically alter a fluid flow. In their study, a giant pulse ruby laser beam fired into a pendant droplet of chlorobenzene containing TNBSP produced violent disturbances in the droplet. Disturbances were attributed to tiny gas bubbles created along the path of the laser beam in the fluid.

Humphrey, Hummel, and Smith [11] adapted a commercial multipulse nitrogen laser to replace the xenon flashtube used to excite the photochromic dye. The flow visualization technique was used to obtain flow patterns inside of growing droplets of solvents in an immiscible ambient fluid. Equations were given to facilitate the computation of velocity profiles in droplets from dye traces. Correcting errors in these trace positions induced by optical refraction were discussed in reference [9]. It was shown that errors in trace position could be very large if the effects of refraction were ignored. Reference [11] contained computed velocity vector distributions along the central core of a slowly growing droplet of an organic liquid in water. The sparse distribution of points sampled within the droplet allowed approximate pressure profiles to be computed.

In Culbreth, Johnson, and Marschall [12], a custom built pulsed nitrogen laser and photochromic dye were used to study droplets of mineral spirits rising in water as part of a study of direct-contact heat transfer. High speed movies at 400 frames per second were made of developing droplets as the pulsed laser produced violet traces in the droplet interiors. The laser design was used in the present work and consisted of a high-voltage power supply, a source of pressurizing nitrogen gas, a vacuum pump, the laser channel made up of plexiglas box with copper electrodes and associated electronics.

A brief history of the pulsed nitrogen laser used for this study begins with the development of an inexpensive, powerful, portable device by James Small reported in reference [13]. His simple laser design involved discharging two copper plates across a 1 cm wide gap in an enclosure containing nitrogen gas at 100 torr of pressure. The two plates were separated by several sheets of mylar plastic dielectric above a ground plate. The upper plates were charged initially to approximately 20000 volts and one plate was periodically grounded producing rapid discharges of electrons through the enclosure containing the nitrogen gas. Collisons between electrons excited the nitrogen gas into emitting photons with a wavelength of 3371 Angstroms. Photon emission occurred in pulses 9 nanoseconds in duration during which 50 to 100 kilowatts of ultraviolet radiation were released. The design described in reference [13] relied on a spark gap to periodically ground out one of the upper plates and, subsequently, fire the laser. Commercial lasers capable of producing pulses of light at these intensities and wavelength cost typically on the order of $10000. In reference [2], the construction of a small pulsed nitrogen gas laser is described costing about $30.

Details of the laser constructed for the present study are discussed later. The spark gap used to fire the laser described above was replaced by a thyratron tube and its

associated electronics as described by Devlin [10]. Devlin developed a liquid cooled pulsed nitrogen laser for non-linear spectroscopic measurements.

The history of the pulsed nitrogen-laser/photochromic dye flow visualization technique has been described. The method appeared to be of value in studying a wide range of fluid dynamics problems where non-intrusive velocity measurements are desired. A facility has been developed here at NPS as a part of this work using this measurement technique and the strengths and weaknesses of the technique as a measurement tool have been assessed. Velocity distributions have been obtained in growing droplets and the necessary computer codes for digitizing and reducing data are presented. The equations necessary for correcting optical distortion and for computing the velocity vectors from dye traces are given. Construction, operation, and safety considerations are explained for the pulsed nitrogen laser built for this project.

III. EXPERIMENTAL PROCEDURE

The apparatus shown in Figure 1 consisted principally of a vertical 3"x3"x10" flat wall, plexiglas, rectangular parallelpiped containing the continuous phase (water). The whole of the experimental equipment was constructed of plexiglas and PVC tubing. Contamination of the system by dust and surface active agents such as chemicals and grease was carefully avoided. Droplets of mineral spirits were formed from a single polished plexiglas nozzle immersed in the continuous phase. The nozzle was pointed so that the dispersed phase did not wet the nozzle tip; therefore, the nozzle diameter could be considered constant. A variable speed positive displacement pump was used to circulate the dispersed phase (mineral spirits) through the system. The flow rate through the nozzle was regulated by a combination of pump speed, recirculation valve position, and cutout valve position. A fluidic capacitor was placed in line downstream of the pump and upstream of the flowmeter as shown in Figure 2 to dampen the pulses that were generated by the pump and to provide a storage area for the mineral spirits. The flow rate was measured using a previously calibrated flowmeter. The mineral spirits was recirculated through the system until equilibrium temperature was achieved and the flow rate steadied out at a previously

selected rate. Upon formation, the droplets were exposed to the ultraviolet radiation produced by the nitrogen laser. The ultraviolet light from the laser was focused through a 12 cm focal length lens until only a very thin laser line was focused in the droplet just above the nozzle exit. Focusing of the laser beam was easily accomplished by putting a few drops of florishene in the water and running the laser at a very high frequency. This allowed a visual check on both the focus of the beam and the exact position that the beam hit the droplet. Upon irradiation of the droplet, the trace was present throughout the entire history in a plane containing the axis of symmetry of the drop. A high resolution television camera focused through a 10 power microscope was used to see the droplet and subsequent laser traces as they were formed. A polaroid picture was taken of the television monitor to record the laser traces. Flow rates were varied and frequency of the laser was varied to obtain the best overall "picture" of the forming drop.

IV. NITROGEN LASER

A. DESIGN CONSIDERATIONS

This thesis required the use of a high powered ultra-violet nitrogen pulsed laser to cause the photochromic dye to change color. The wavelength of the laser output was 337.1 nm with peak power of 200-300 megawatts within a pulse width of approximately 9 nanoseconds. The pulsing frequency was variable so that at low flow rates, the droplets would not saturate causing the laser traces in the droplet to merge. A choice of a high voltage thyratron to discharge a capacitor was therefore made.

B. LASER PRINCIPLES

The basic design criteria for a nitrogen laser is to excite as many molecules as possible and to do it in a short period of time (10 nanosec). The closely spaced group of laser transitions near 337.1 nanometers in the nitrogen molecule may be thought of as arising from a simple four level electronic group. See Figure 3. An electron in the nitrogen molecule is promoted from the ground state to the upper laser level by a collision with a free electron in the high voltage discharge. The molecule then relaxes to the lower laser level emitting a quantum of light at the 337.1 nanometer wavelength. A very high voltage is used to pump the nitrogen molecule up to the upper laser level. The

laser chosen consisted of two 25 cm long parallel copper plates separated by a 1 cm gap. A rectangular plexiglas enclosure was placed around the plates near the gap. The enclosure was filled with nitrogen gas at low pressures to provide the lasing medium. Glass microscope slides with a thickness of 1.33 mm were attached to both ends of the enclosure to allow the laser beam to pass out of the enclosure. The laser plates were separated by a thin mylar sheet with a high dielectric constant from a ground plate. The plates were configured as capacitors by an electronic circuit first described by Blumenthal [2]. By pulsing very high voltages across the gap between the two copper plates surrounded by nitrogen gas, the gas was bombarded by electrons producing the plasma which emitted a quantum of light in the ultraviolet range. The surface area of the copper plates determined the magnitude of the output signal. The larger the surface area, the larger the capacitance resulting in a larger output signal. However, increasing the area caused the time to charge the plates to increase.

C. LASER CONSTRUCTION

1. Laser Channel

The copper electrode plates of the capacitor are an integral part of the laser channel. Figure 4 shows the dimensions of the electrode plates. Plates of 6.35 millimeter thick plexiglas were used to construct all the sides

of the laser channel. This reduced the amount of ultraviolet light emitted to the surrounding area since the plexiglas absorbed all of the ultraviolet light produced by the laser that did not go through the output windows. The dimensions of the plexiglas sides are shown in Figure 5. Figure 6 shows how the plexiglas pieces and the electrode plates go together to form the laser channel. A front surface mirror was placed at the back of the laser channel to double the intensity of the laser output by reflecting the ultraviolet light back through the laser channel and out the front window. Silicon sealer was used to seal all joints and make the laser channel vacuum tight.

2. Capacitor

The capacitor was made from thin copper plates and layers of 0.0075 inch thick mylar plastic sheets. Figure 6 shows how the capacitor was assembled. The thyratron lead was soldered to the top capacitor plate and a ground strap was soldered to the bottom left capacitor plate. The assembled capacitor was then bolted together using phenolic particle board to hold the copper plates and mylar sheets tightly together. The measured capacitance was found to be 0.0045 microfarads. Details of the final assembly are shown in Figure 7.

3. Electronics

This laser design utilized an EG&G HY1102 grounded grid thyratron. Its placement in the laser circuit is shown in Figure 8. All electronic components were installed in a cart underneath the laser channel to limit the lengths of the high voltage leads to the laser channel and to make the laser semi-portable. Figures 9 and 10 show the details of the triggering circuits for the thyratron.

4. Laser Container

The laser components were installed in the cart as shown in Figure 11. This cart was grounded to provide the operator protection from high voltages and any static electricity buildup. The cart also attenuates any Radio Frequency energy generated by the electronic components.

D. AUXILIARY SYSTEMS

1. Vacuum System

A Welch model 1402 DUO-SEAL vacuum pump was used to maintain the laser channel between the ideal 26-28 inches of vacuum. The suction line was installed at the rear of the laser channel and a 0-30 inch Hg vacuum gauge was placed between the laser channel and the vacuum pump close to the laser channel.

2. Nitrogen Gas Supply

Nitrogen gas was supplied to the front of the laser channel via a reducing valve and cutout valve. Nitrogen

pressure to the cutout valve was set for 10 psi and the cut-out valve was used to regulate the laser channel pressure.

3. Power Supplies

The thyratron reservoir filament and cathode filament heaters were powered by a 115 v AC voltage source through a transformer which reduced the voltage to 6.2 volts. The SCR anode voltage was supplied by an HP 711A 0-300 VDC power supply. A WAVETEC pulse generator provided the +/- 10 V square wave signal at various frequencies to the cathode decoupler network. High voltage was supplied by a HIPPOTRONICS 0-30 kV power supply. Power supply connections are shown in Figure 8.

E. LASER OPERATION

1. Operational Settings

The SCR anode voltage was set to 250 volts. The pulse generator was at the desired frequency between 1 and 30 Hertz. Channel pressure varied between 2-4 inches absolute of mercury. Alignment of the output mirror was done by removing the mirror and sighting down the laser channel to the target. The mirror was installed and sighting down the laser channel in the opposite direction allowed for its alignment.

2. Firing Sequence

An understanding of the firing sequency is essential to the safe operation of the electronic circuitry.

Initially the top capacitor plates are charged to a voltage of about 18,000 V and the bottom plate is grounded. A large negative pulse is applied to the thyratron cathode. This large negative pulse causes a discharge between the thyratron grid and anode. After discharge, the top left capacitor plate becomes negatively charged with respect to the top right capacitor plate. A high potential between the two electrode plates will result in breakdown and thus excitation of the nitrogen molecule by electron collisions. An inductor is placed in line between the left and right capacitor plates to allow the charge buildup to occur on the right top plate and to allow the right top plate to ground completely before the next pulse is applied to the left plate.

3. Turn-On Procedure

a) Plug in the power cord for the thyratron heater elements. A 10 minute warmup time is required to prevent damage to the thyratron when operating.

b) Evacuate the laser channel.

c) Connect the 67.5 VDC battery to the terminals.

d) Adjust the nitrogen gas supply to maintain 26-28 inches Hg vacuum in the laser channel.

e) Set the SCR anode voltage for 250 Volts.

f) Turn on the pulse generator and set to the desired frequency.

g) Energize the high voltage power supply. Slowly raise the voltage until lasing occurs at approximately 15 kV. Do not exceed 20 kV. The thyratron can be damaged if the voltage exceeds 20 kV. NOTE: The high voltage will increase as pulsing frequency decreases.

4. Turn-Off Procedure

To turn off the laser follow the turn-on procedure in reverse order. It is important that the high voltage be lowered before lowering the frequency because you can exceed 20 kV. Turn off the nitrogen supply and let the pressure bleed down before turning off the vacuum pump to eliminate the possibility of creating a pressure inside the laser channel greater than atmospheric. This situation can lead to pinhole leaks forming in the laser channel.

F. LASER SAFETY

Ultraviolet radiation can cause serious damage to the operator's eyes. To reduce the hazard, the laser was set up in a controlled access area. Only those people wearing plastic safety glasses were allowed in the room while the laser was in operation.

Since very high voltages were used, the laser container was grounded to prevent a shock hazard. It also prevented a static electricity buildup on any components.

V. DATA ANALYSIS

The photograph showing the clearest laser traces was digitized using an HP-9845 computer system. Figure 12 shows the data points used in the analysis.

The first step was to correct all the data points for the difference in refraction between the mineral spirits and water. The correction is necessary because a curved surface separating two medias of different indices of refraction will cause the apparent displacement of any point within one or the other mediums when viewed through the interface.

A. ASSUMPTIONS

The following assumptions are made:

1) The drop is symmetrical about its vertical axis and its profile can be accurately described by the empirical equation given by Poutanen and Johnson [2] for growing bubbles.

$$R^n \vartheta = 1 \qquad (2)$$

where: R, ϑ = polar coordinates of the profile

n = arbitrary parameter chosen to fit any particular droplet

Figure 13 shows the drop geometry for Equation (2).

2) The point object is located in a plane containing the drop axis; the said plane being perpendicular to the normal of the camera lens.

3) All rays of light proceeding from point objects within the drop, upon crossing the interface can be assumed to follow paths parallel to the normal of the camera lens.

4) The center of gravity of the growing drop and the camera lens central axis remain at the same height during drop growth.

B. CALCULATION OF OPTICAL DISPLACEMENTS

The direct application of Equation (2) in polar form is very inconvenient for the present analysis. A transformation into the Z-Y coordinate system was made taking the apex of the drop as the origin. The result of the transformation is:

$$(Y^2 + Z_1^2)\,\mathrm{ARCTAN}\left(\frac{Y}{Z_1}\right) = 1^n \qquad (3)$$

where:

$$Z_1 = Z - R_o \qquad (4)$$

$$1 = D_m/d' \qquad (5)$$

R_o = distance from the polar coordinate origin to the new origin

n, d' = empirical constants determined as in [9]

It can be shown that the optical corrections can be expressed as:

$$\Delta Z = \text{TAN}(\hat{r}-\hat{i})\ \sqrt{C^2-R_2{}^2/\text{TAN}(\hat{r})} \qquad (6)$$

$$\Delta Y = (\text{TAN}(\hat{r}-\hat{i})/\text{TAN}(\hat{r}))\ x\ R_2 \qquad (7)$$

where:

$$\hat{r} = \text{ARCOS}(C/(R_1\ \sqrt{1+(1/m_1)})) \qquad (8)$$

$$\hat{i} = \arcsin(n_r/n_i\ \text{SIN}(\hat{r})) \qquad (9)$$

$$C = \sqrt{R_1{}^2 - R_2{}^2} \qquad (10)$$

R_1 = Distance from center to edge of bubble.

R_2 = Distance from center to edge of point to be corrected.

n_r = Index of refraction of water

n_i = Index of refraction of mineral spirits

$$m_1 = \frac{(Z_f-R_o)(R_1{}^2+(Z_f-R_o)^2)^{\frac{N+2}{2}}\cos^2(\ell^N(R_1{}^2+(Z_f-R_o)^2)^{-N/2})+n\ell^n R_1(Z_f-R_o)^2}{R_1(R_1{}^2+(Z_f-R_o)^2)^{\frac{N+2}{2}}\cos^2(\ell^N(R_1{}^2+(Z_f-R_o)^2)^{-N/2}) - n\ell^N(Z_f-R_o)^3} \qquad (11)$$

Z_f = Vertical coordinate of point F

The optically corrected data points are then determined by:

$$X = X \pm \Delta Y \qquad (12)$$

$$Z = Z \pm \Delta Z \qquad (13)$$

Figure 14 shows the position of the corrected data points. Figure 15 shows the position of the corrected and uncorrected

data points. Figure 18 is the HP-9845 computer program that was used to solve the above equations for the optical corrections.

C. VELOCITY VECTOR DETERMINATIONS

Due to symmetry, only the right half of a droplet need be considered as shown in Figure 16. The Y axis lies along the center line of the nozzle and is given the value 0 at the nozzle exit, Y is positive in the direction of flow. The radial coordinate is labeled X, and is positive away from the centerline.

Quantitative measurements of fluid flow inside the droplet were limited to a core along the Y axis with the same diameter as the inside diameter of the nozzle. In this well defined region, the shape of any induced trace i, after correction for optical distortion, was found to be excellently represented by a polynomial of degree 3 i.e.,

$$F(X) = a(I)X^3 + b(I)X^2 + c(I)X + d(I) \qquad (14)$$

where a(I), b(I), c(I), and d(I) are time dependent and are calculated by a least squares fit of Equation (14) to the experimental values.

The fact that flow within the growing droplet is not undirectional except at very high flow rates complicates the calculation of fluid element velocities from the induced traces. Two traces within the drop at time t are shown as

dotted lines in Figure 16. At a later time $t+\Delta t$, the same traces are shown as continuous lines. It is possible to follow the change of position of an element of fluid from point A to point B using a mass balance technique as follows. Consider the displacement of an element of fluid (P1, P2, P3, P4) contained between traces 1 and 2 during an interval of time Δt as shown in Figure 16. As the element moves forward to its new position it is distorted, some of the fluid from the moving element being squeezed out in the radial direction. Provided the fluid element is small, an approximation to its vector velocity is:

$$V = \overline{AB}/\Delta t \tag{15}$$

and the direction of its movement can be characterized by the angle α.

Given trace 1 and 2,

Let A_X = X coordinate of point A

Let A_Y = Y coordinate of point A

Then

$$A_Y = 1/2[(a(2)-a(1))A_X^3+(b(2)-b(1))A_X^2 + (c(2)-c(1))A_X + d(2)-d(1)]+F(A_X) \tag{16}$$

Though distorted due to a combined radial and axial motion of the fluid, the volume of the fluid element remains the same during an interval of time Δt. Since the trace containing the distorted element can also be fitted to

equations of the type given by Equation (14), where the constants are now found for that element of volume, the volumes are set equal to each other and the polynomial is solved for the X coordinate of point B. Therefore from the theorem of PAPPUS:

Let B_X = X coordinate of point B

Let B_Y = Y coordinate of point B

$$V(1,2) = (a(2)-a(1))A_X^5 + (b(2)-b(1))A_X^4 + (c(2)-c(1))A_X^3 + (d(2)-d(1))A_X^2 \qquad (17)$$

$$V(3,4) = (a(4)-a(3))B_X^5 + (b(4)-b(3))B_X^4 + (c(4)-c(3))B_X^3 + (d(4)-d(3))B_X^2 \qquad (18)$$

Now, since V(1,2) = V(3,4) Equation (18) can be solved for B_X. Once this value is found, substitution into the following equation gives B_Y.

$$B_Y = 1/2[(a(4)-a(3))B_X^3 + (b(4)-b(3))B_X^2 + (c(4)-c(3))B_X + (d(4)-d(3))] + F(B_X) \qquad (19)$$

The velocity can now be expressed as:

$$V = \sqrt{(B_X-A_X)^2 + (B_Y-A_Y)^2} \qquad (20)$$

and the angle α can be found by:

$$\alpha = \text{ARCTAN}((B_Y-A_Y)/(B_X-A_X)) \qquad (21)$$

Figure 19 is the HP-9845 computer program that was used to solve the above equations for the velocity vectors and angles.

VI. RESULTS

Figure 17 shows the velocity profiles for the 4 traces that were obtained during this procedure. As can be seen, the velocity decreased as the fluid moved away from the nozzle in the vertical direction; and the velocity along a given trace also decreases as you move away from the centerline. The magnitude of the peak velocity coming out the nozzle was computed to be 97.6 micrometers per second. This corresponds to a Reynolds number of approximately 0.05. The velocity profile looked very much like the laminar velocity profile at the nozzle exit which is parabolic in shape. Table I shows the coordinates and magnitude and direction of the velocity vectors using laser traces 1-2, 2-3. The origin of the coordinate system is the center of the nozzle at the nozzle exit. The magnitude of the velocity is unitless and is equal to the computed velocity divided by the peak velocity in the nozzle. Likewise, Table II shows the results using laser traces 2-3, 3-4 and Table III shows the results using laser traces 1-3, 2-4.

A. ERROR ANALYSIS

All positional measurements in the droplets were based on the observed nozzle bore diameter. The accuracy of the bore diameter was approximately 2.7%. The droplet profiles and position of points on traces were digitized from a polaroid picture of droplets obtained through a videoscreen. The effects of parallax were minimized by placing the camera as far from the inlet nozzle as possible. Humphrey and Hummel [9] reported that parallax error is negligible if the droplet traces are observed from more than 25 cm and readings are confined to within 3 mm of the center of gravity of the droplet. In this study, the camera was placed approximately 15 cm away from the droplet and traces were viewed within 1 mm of the droplet center. The error caused by the nozzle bore diameter far exceeded the digitizing error of 0.008 mm.

The error induced in determining each point on a trace in (X,Y) coordinates was influenced by errors in maximum droplet diameter, point coordinates R_2 and Z_F described earlier, and the indices of refraction of mineral spirits and water.

The errors in indices of refraction were assumed to be small and in the correction for optical refraction, positional errors predominated. An analysis was done to compute the error in position for points on the traces in the

droplets after correcting for refraction. The uncertainty analysis technique detailed by Holman [14] was used. The points obtained from photochromic dye traces that were used to compute velocities were all confined within an area no wider than the inlet nozzle diameter and far from the apex of the droplet. Within this area, point positions were known within $\pm$ 0.005 mm after correcting for refraction.

The corrected traces were curve fitted using a third order polynomial. The fit was very good with a standard deviation of under 0.001 mm. The time interval between firings was accurately controlled by a crystal based function generator with an accuracy of about $\pm$ 0.0001 seconds. All computations on the HP-9845 were done in double precision arithmetic to minimize errors.

The estimated accuracy of the fluid velocities was, on the average, 0.07 mm/s or 6.3% of the average fluid velocity at the nozzle tip.

It should be noted that errors will rise very rapidly if data is taken near the periphery of the droplet due to the traces appearing to be very close to one another.

VII. CONCLUSIONS

Velocities were computed using a nitrogen laser/flow visualization technique. The technique was used to investigate the velocity profile in the core of a slowly forming droplet (Re = 0.05). Velocities along the centerline of the droplet were seen to decrease from a peak velocity in the nozzle of 2.22 mm/s to 95.6%, 87.8%, and 68.1% of the peak velocity as one moves toward the droplet apex. Peak velocity in the nozzle equaled twice the average velocity as determined from parabolic laminar profile in a circular pipe. Computed velocities agreed well with expected velocities and with the restrictions of laminar flow and small flow geometry, this measurement technique appears to be accurate and useful.

VIII. RECOMMENDATIONS

Since a "home-made" laser was used in this experiment, only simple hydrodynamic problems can be solved. The absorption of the laser light by the mineral spirits necessitated the use of a very small diameter nozzle. Only with high powered commercial grade lasers can this technique be expanded to more challenging hydrodynamic problems. Since only polaroid pictures were taken the rate of droplet growth was severely limited. This, in turn, limited the laser frequency so that saturation did not occur.

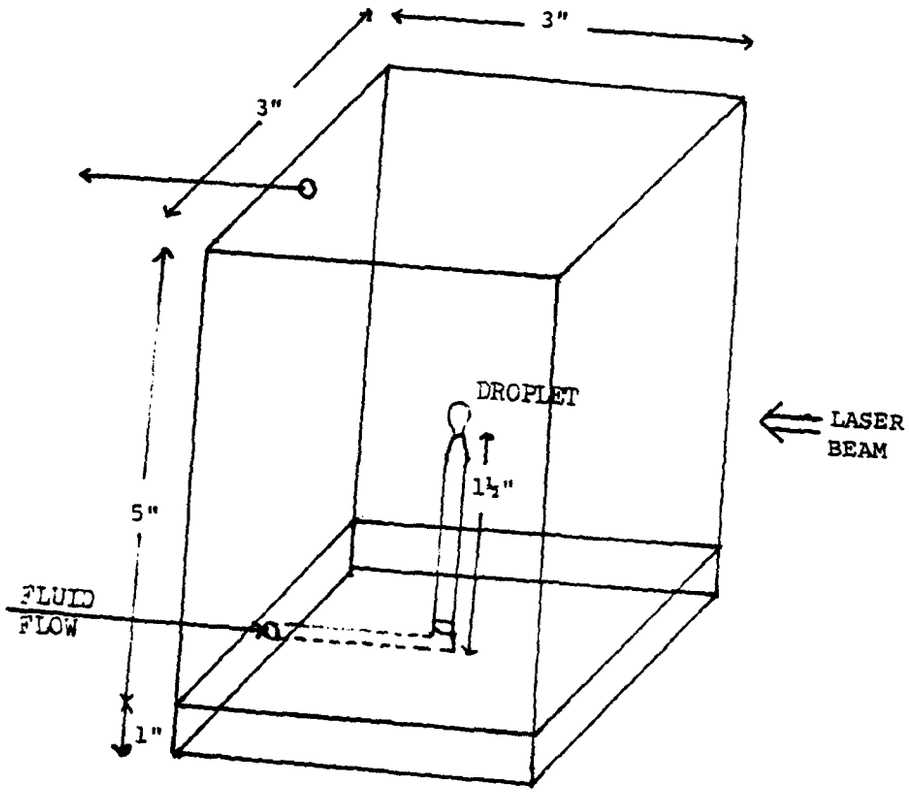

Figure 1

Experimental Test Cell

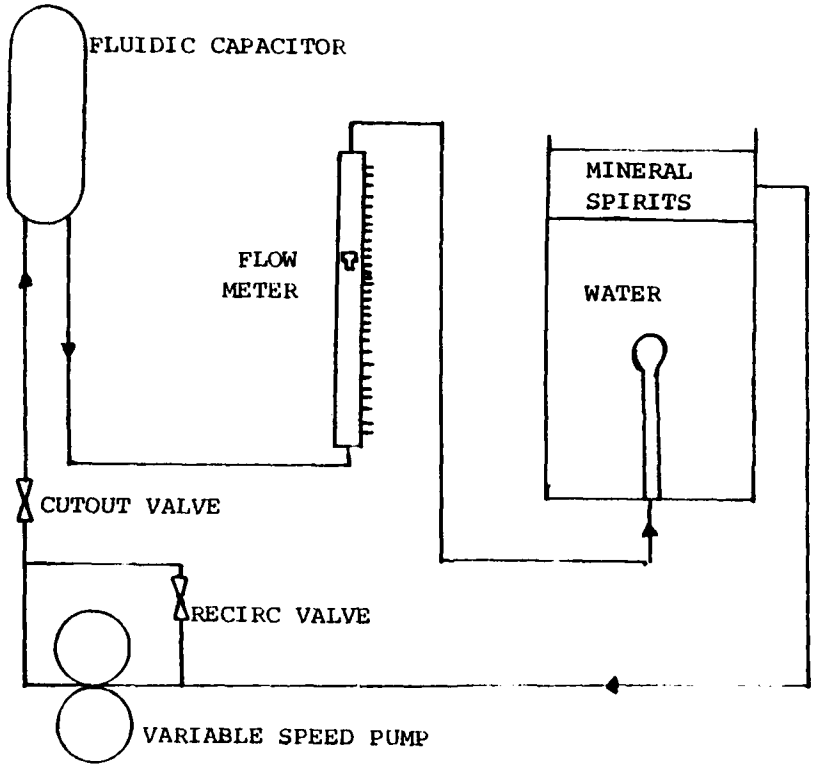

Figure 2

Line Diagram - Test Assembly

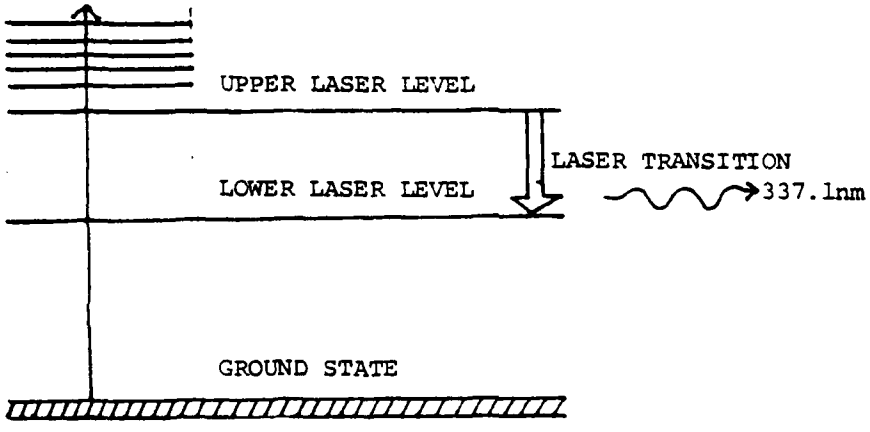

Figure 3

Nitrogen Electronic Excitation Levels

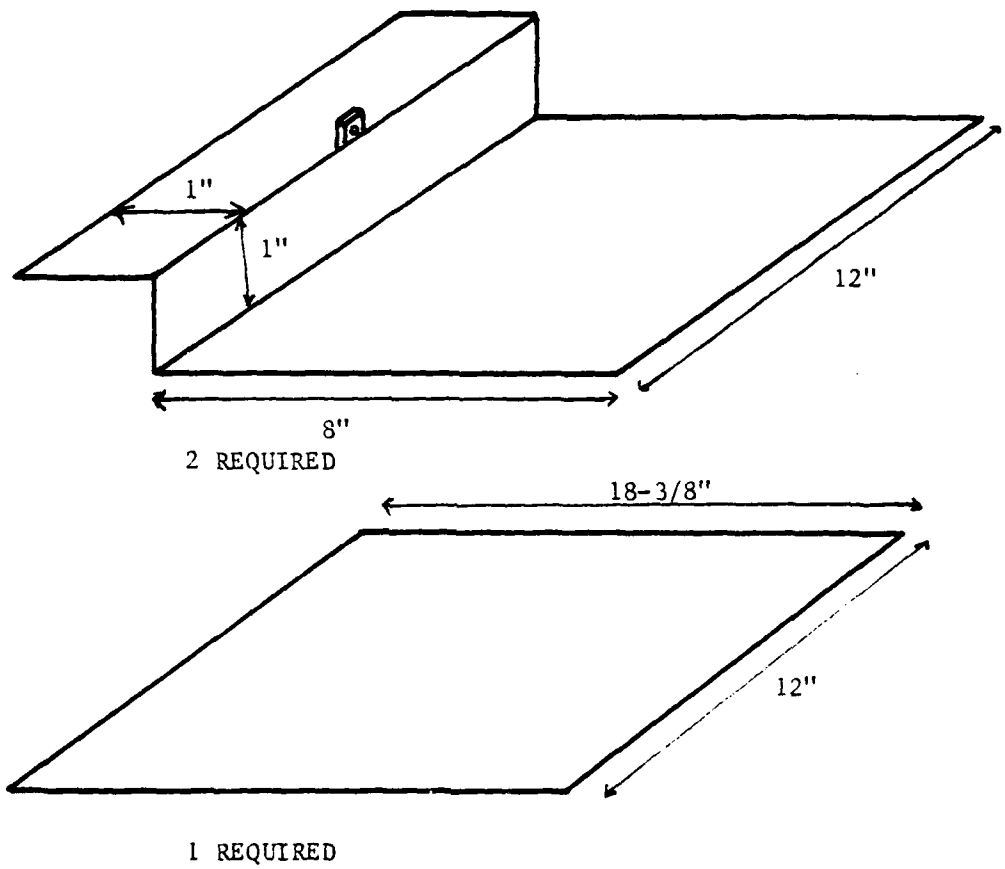

Figure 4

Copper Electrode Plates

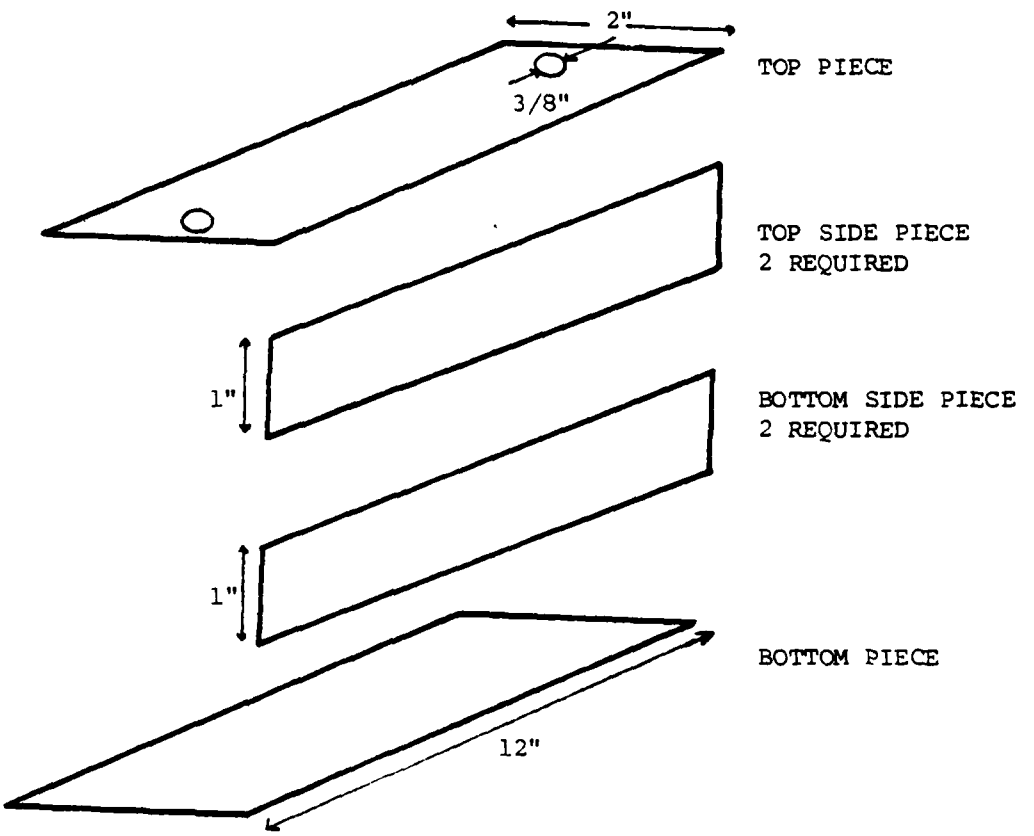

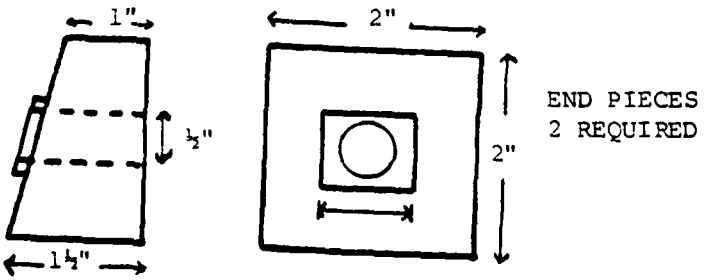

Figure 5

Laser Channel Plexiglas Pieces

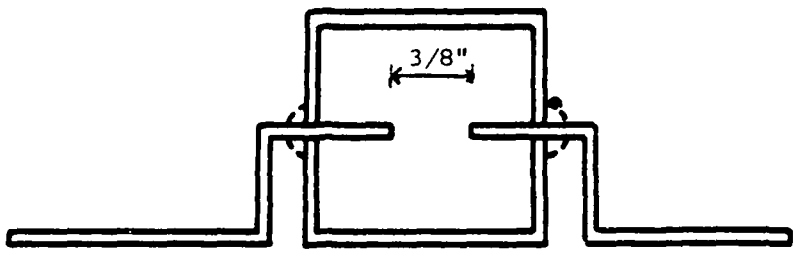

END VIEW

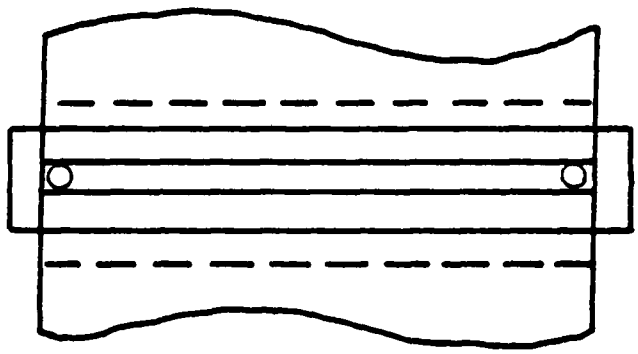

TOP VIEW

OUTPUT
MIRROR

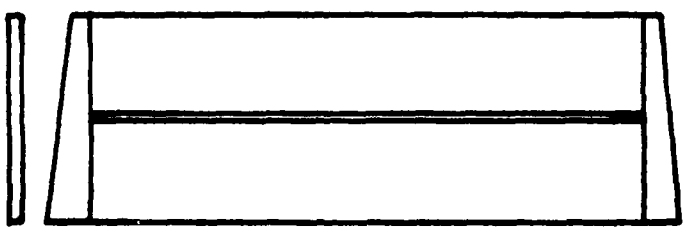

SIDE VIEW

Figure 6

Laser Channel

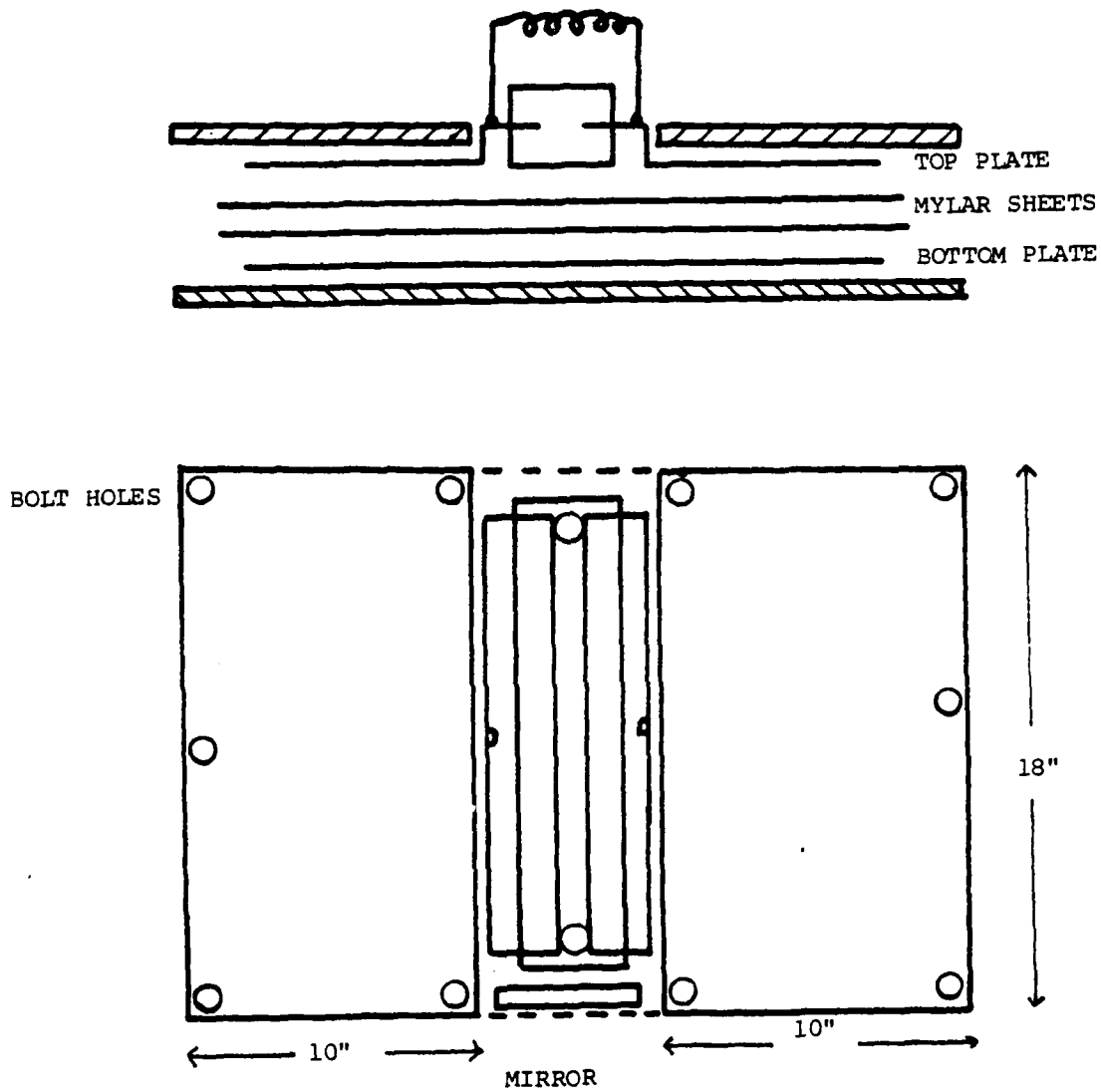

Figure 7

Final Assembly

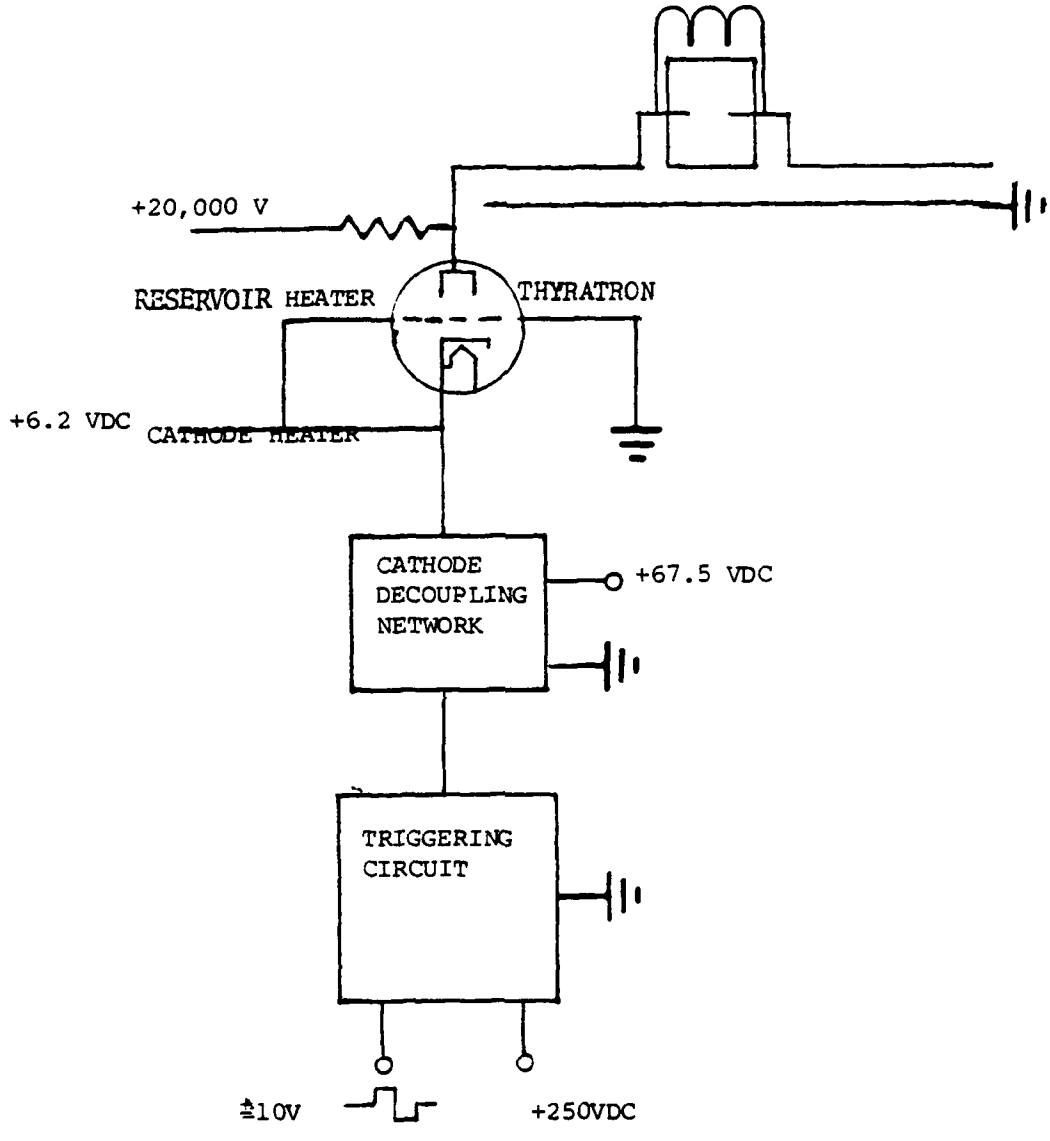

Figure 8

Thyratron Placement in Laser Circuit

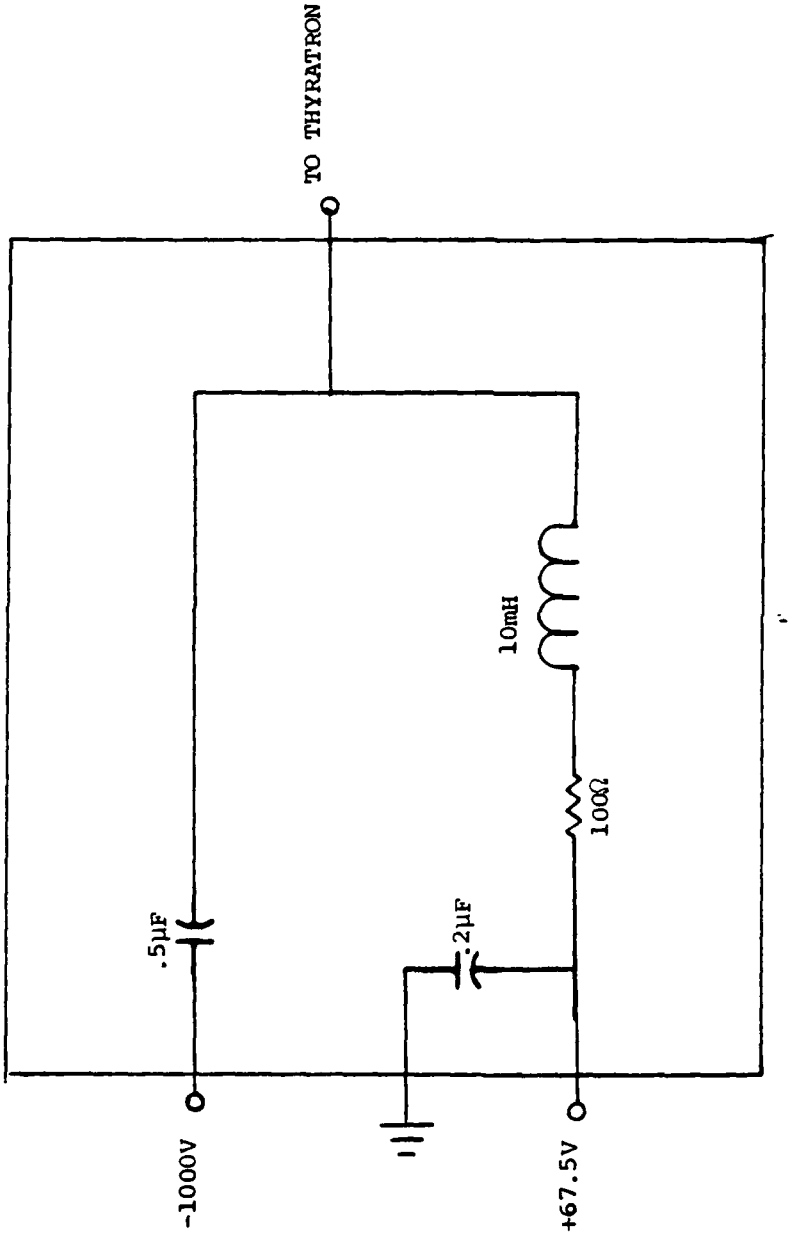

Figure 9

Decoupler Network

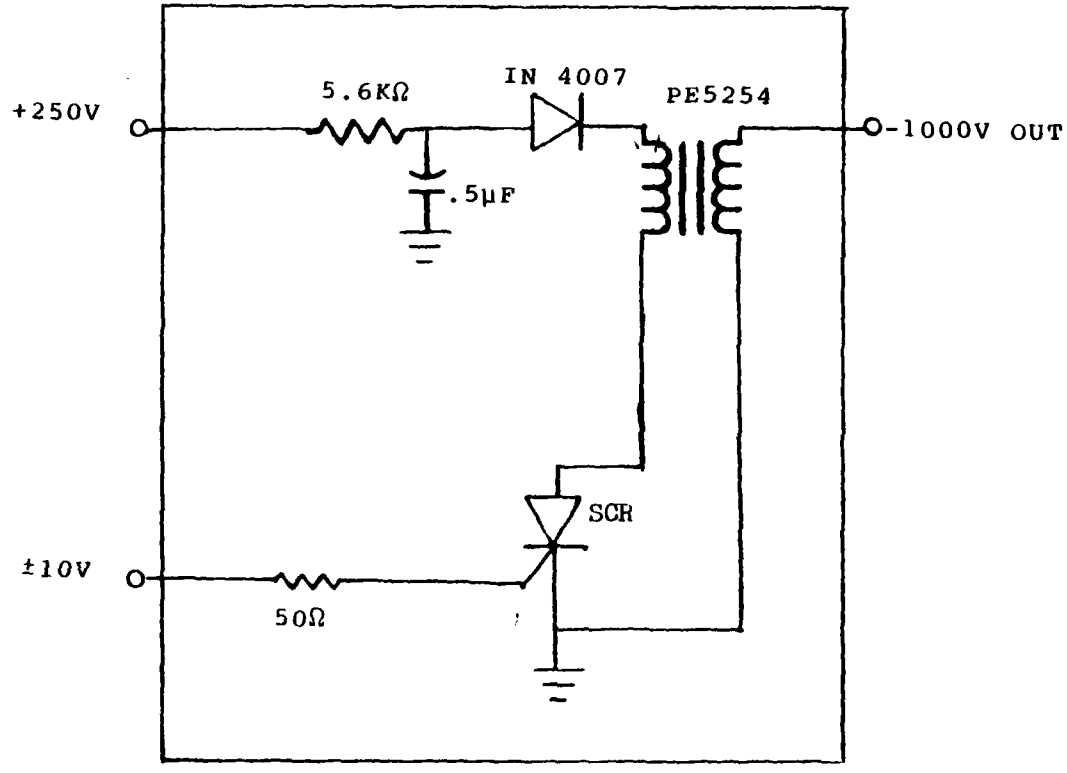

Figure 10

Triggering Circuit

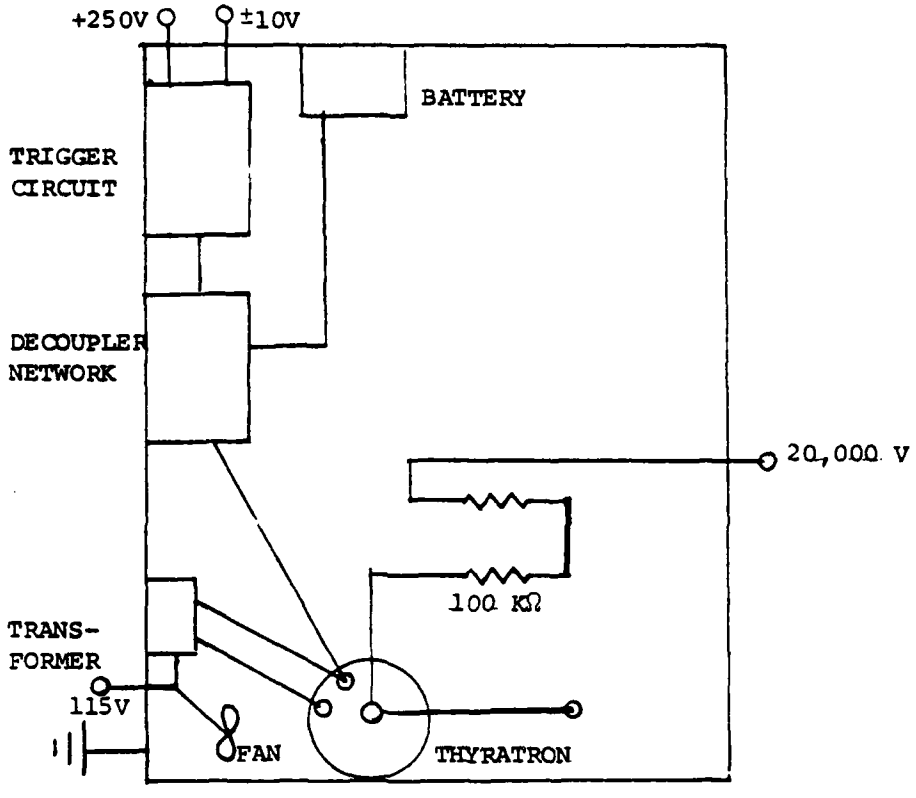

Figure 11

Electronic Component Configuration

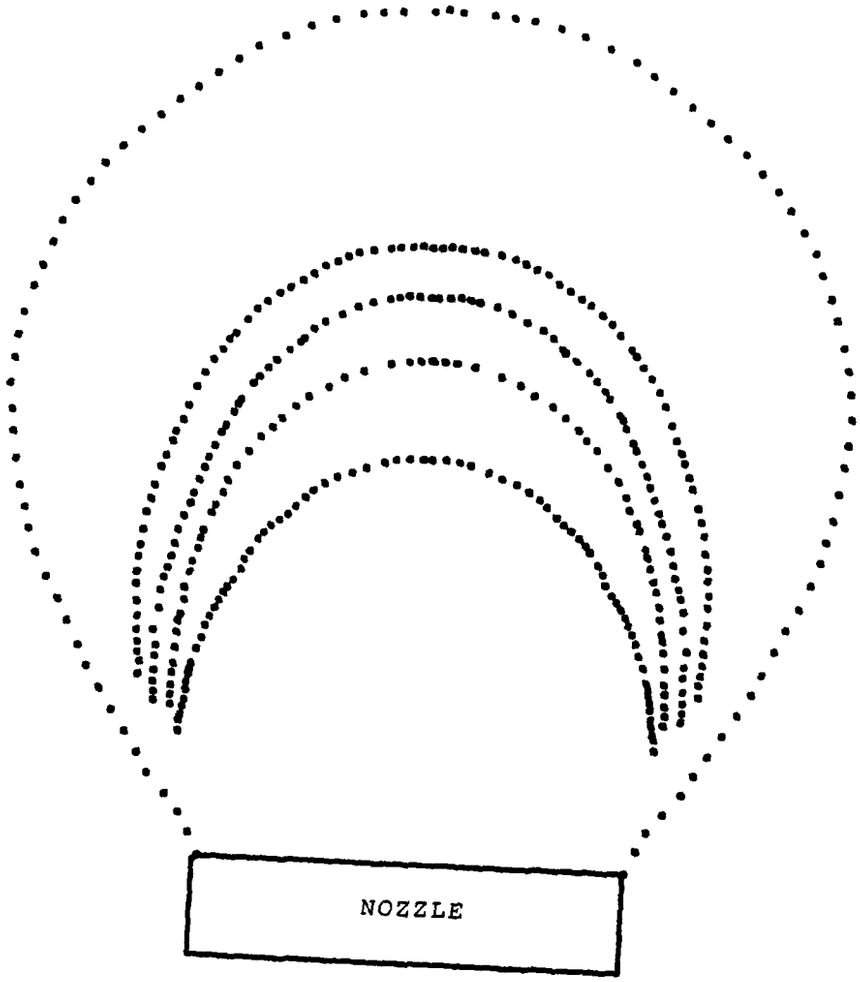

Figure 12

Photochromic Dye Traces in Growing Droplet

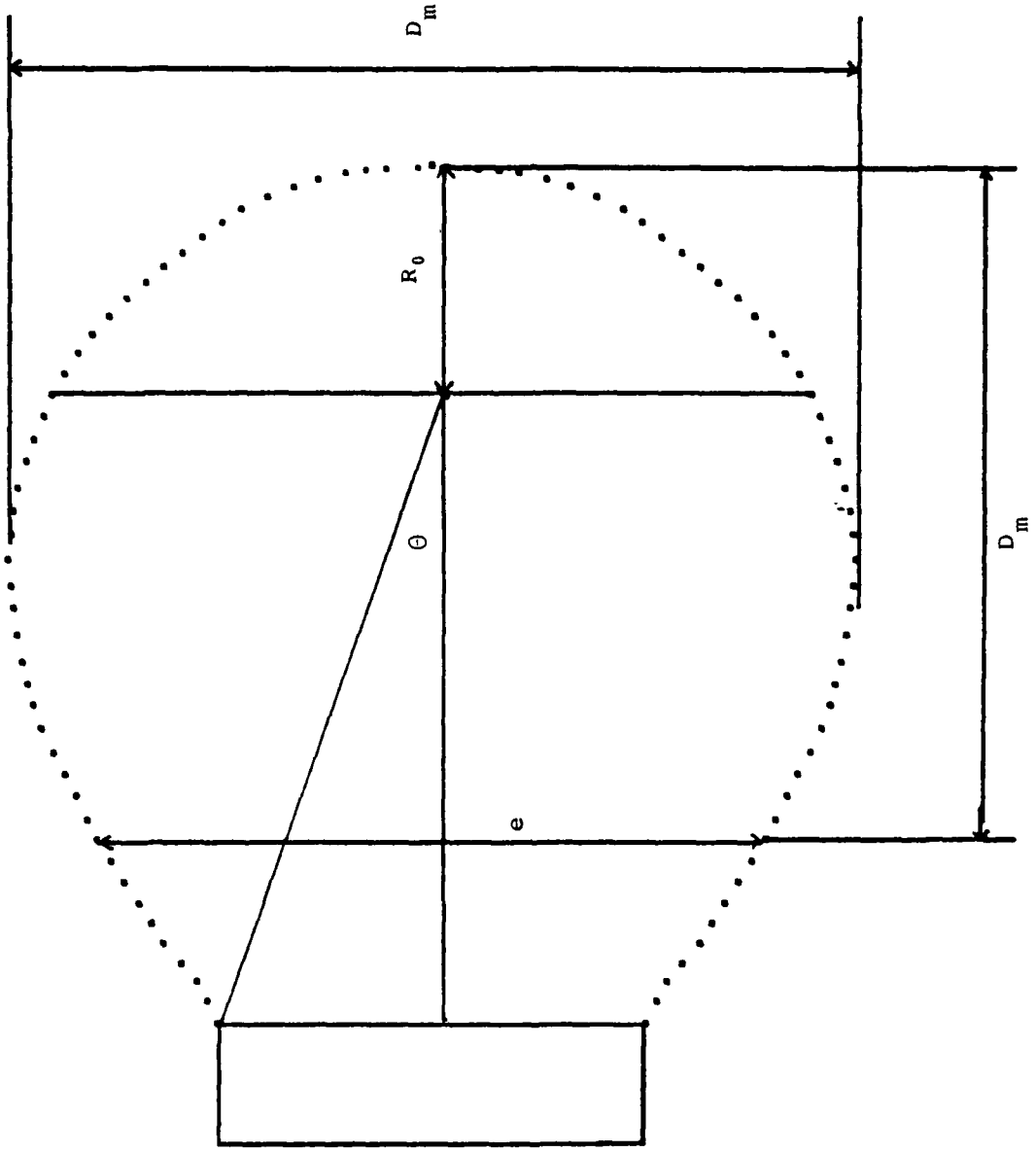

Figure 13

Geometry for Equation (2)

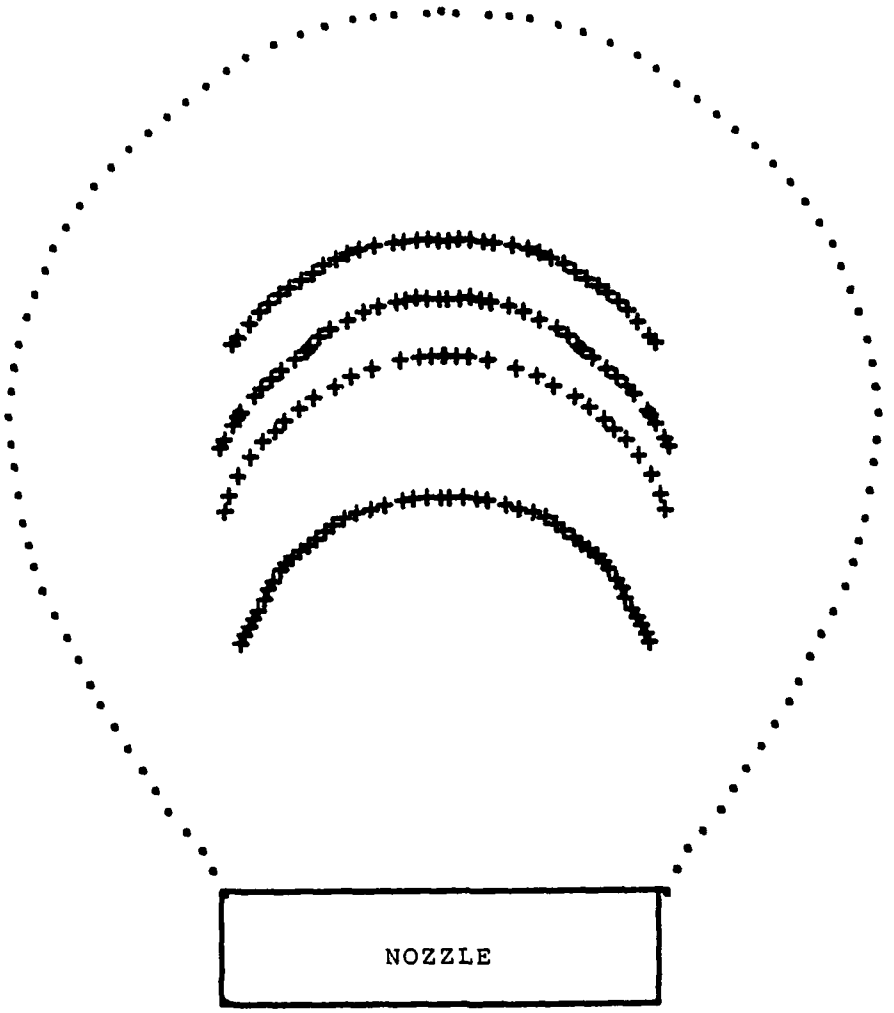

Figure 14

Corrected Data Points

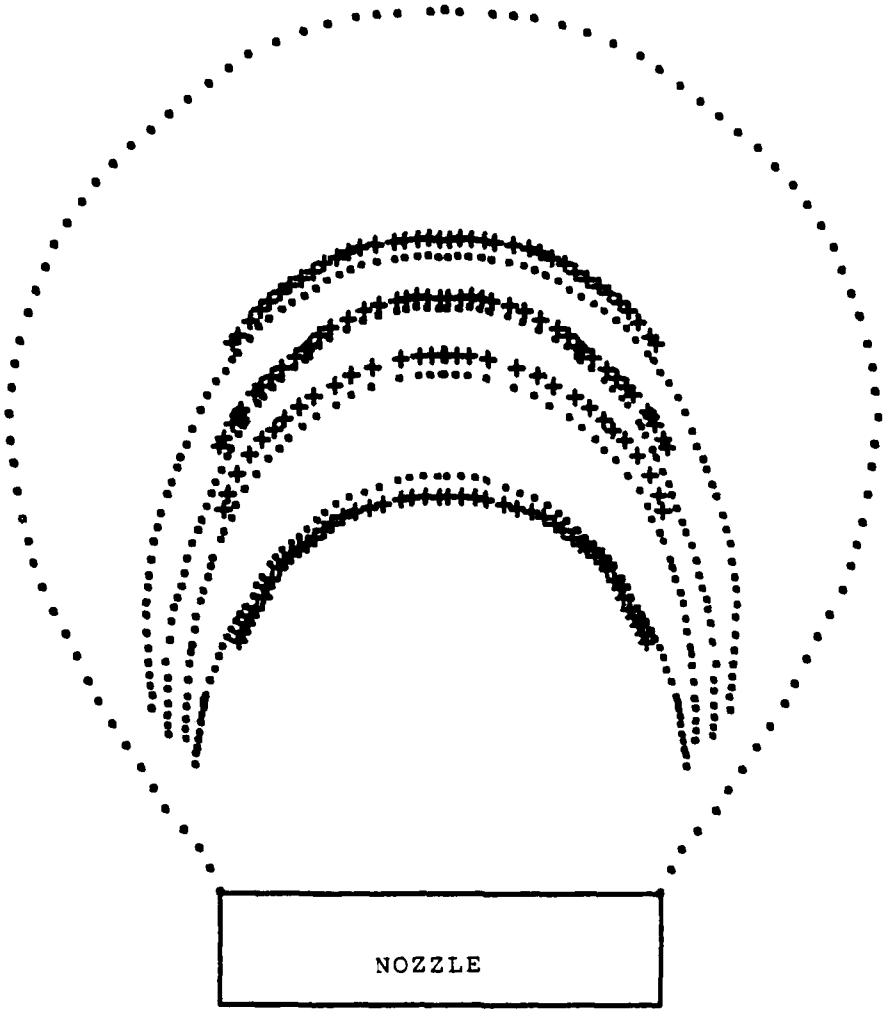

Figure 15

Optically Corrected and Uncorrected Data Points

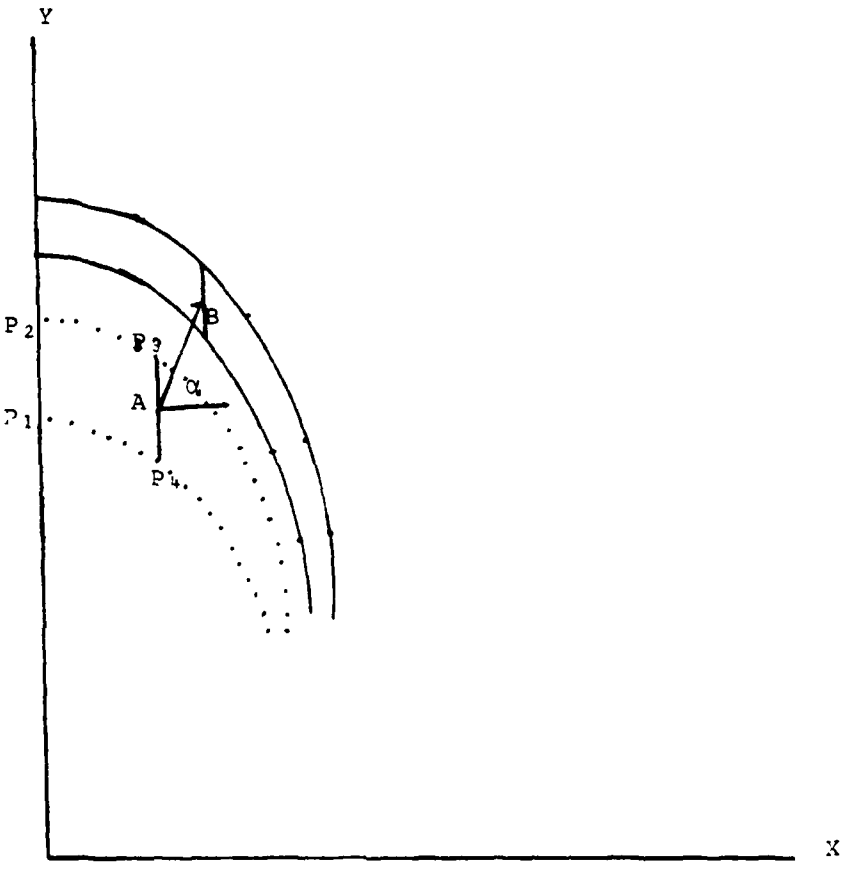

Figure 16

Velocity Vector Computations

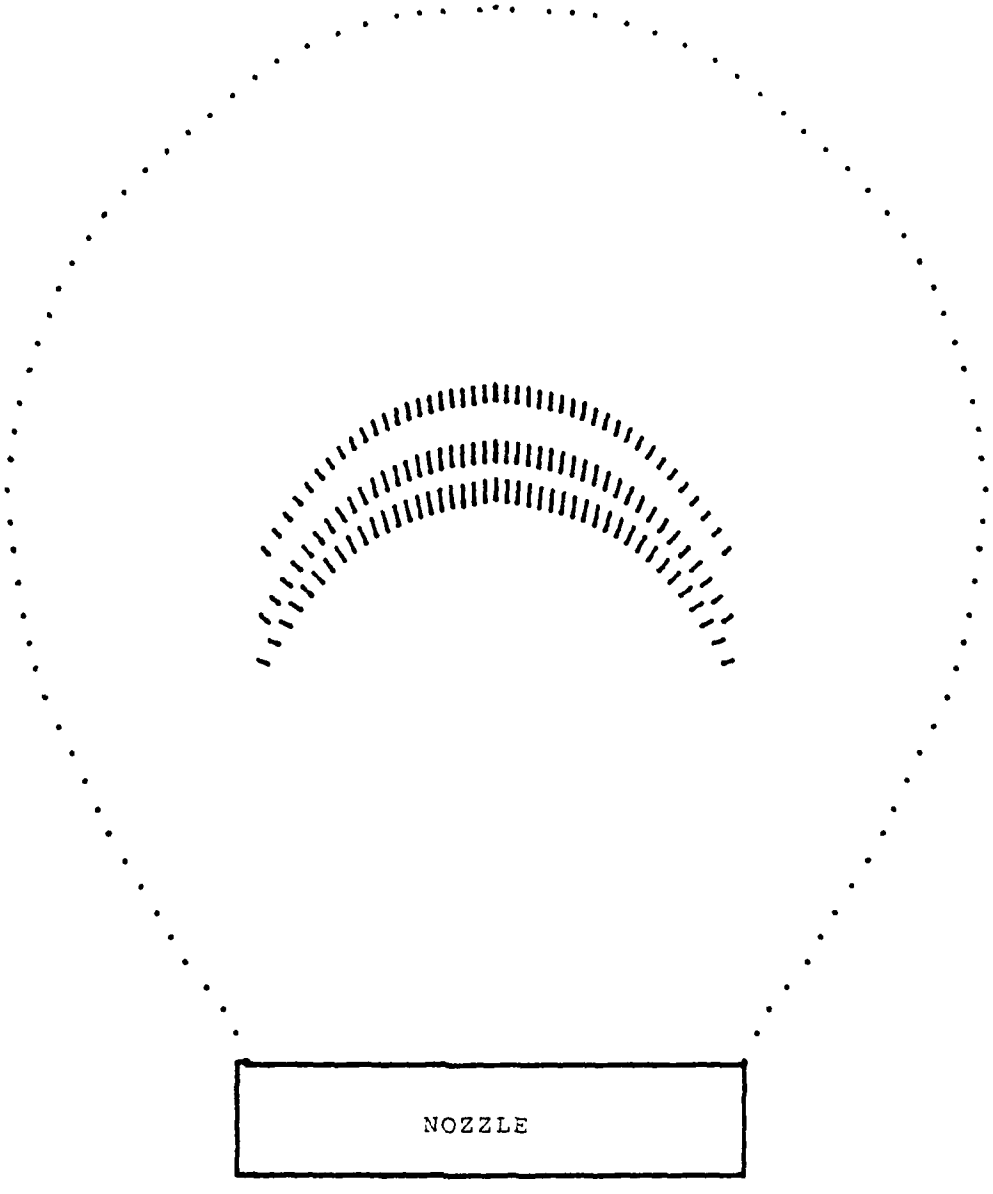

Figure 17

Velocity Profile inside the Droplet

```
10 OPTION BASE 1
11    DEG
20    DIM R2(100),R1(100),Zf(100),X(100),Y(100)
30    ASSIGN #1 TO "BUB1"
40    READ #1,1
50    FOR I=1 TO 24
60    READ #1;X(I),Y(I)
70    R2(I)=X(I)
80    Zf(I)=4039-Y(I)
90    NEXT I
91    ASSIGN #1 TO "R11 :F8,0"
92    READ #1,1
100   FOR I=1 TO 24
110   READ #1;R1(I)
120   NEXT I
130   L=2010
140   N=5.0
150   R0=1608.9
160   Etai=1.48
170   Etar=1.41
180   Delta=L^N
190   CREATE "BUBLE1:F8",1,16*50
200   ASSIGN #1 TO "BUBLE1"
210   READ #1,1
220   FOR I=1 TO 24
230   C=SQR(R1(I)^2-R2(I)^2)
240   Alpha=Zf(I)-R0
250   Beta=R1(I)^2+Alpha^2
251   Q=Alpha*Beta^3.5
260   M0=Q*COS(Delta*Beta^(-N/2))^2
270   M0=M0+N*Delta*R1(I)*Alpha^2
271   Q1=R1(I)*Beta^3.5
280   M2=Q1*COS(Delta*Beta^(-N/2))^2
290   M2=M2-N*Delta*Alpha^3
300   M1=M0/M2
310   Rhat=ACS(C/(R1(I)*SQR(1+M1^(-2))))
320   Ihat=ASN(Etar/Etai*SIN(Rhat))
330   Deltay=TAN(Rhat-Ihat)/TAN(Rhat)*R2(I)
340   Deltaz=TAN(Rhat-Ihat)*SQR(C^2-R2(I)^2/TAN(Rhat)^2)
350   X(I)=X(I)-Deltay
360   Y(I)=Y(I)-Deltaz
370   PRINT #1;X(I),Y(I)
380   PRINT X(I),Deltay,Y(I),Deltaz
390   NEXT I
400   DISP "COMPLETE"
410   STOP
420   END
```

Figure 18

Program to Determine Optical Corrections

```
10 A1=-9.0056E-7
20   A2=-1.00851E-6
30   A3=-5.5438478E-7
40   A4=9.057368E-8
50   B1=.00005203
60   B2=.00031211675
70   B3=-.00027479
80   B4=-.00115860063
90   C1=-.17388898
100  C2=-.25135398
110  C3=-.05371831
120  C4=.23956036
130  D1=1971.8256
140  D2=2425.3585
150  D3=2716.78929
160  D4=2943.295854
170  Z1=A2-A1
180  Z2=B2-B1
190  Z3=C2-C1
200  Z4=D2-D1
210  Z5=A3-A2
220  Z6=B3-B2
230  Z7=C3-C2
240  Z8=D3-D2
250  CREATE "BBVEL1",1,2880
260  ASSIGN #1 TO "BBVEL1"
270  READ #1,1
280  L2=0
290  L1=0
291  DEG
292  BUFFER #1
300  FOR I=1 TO 89
310  Ay=(Z1*L1^3+Z2*L1^2+Z3*L1+Z4)/2+A1*L1^3+B1*L1^2+C1*L1+D1
320  Coef=Z1*L1^5+Z2*L1^4+Z3*L1^3+Z4*L1^2
330  FOR J=1 TO 2000
340  Ck=Z5*L2^5+Z6*L2^4+Z7*L2^3+Z8*L2^2-Coef
350  IF Ck>0 THEN GOTO 380
360  L2=L2+1
370  NEXT J
380  By=(Z5*L2^3+Z6*L2^2+Z7*L2+Z8)/2+A2*L2^3+B2*L2^2+C2*L2+D2
390  Ab=.25+SQR((L2-L1)^2+(By-Ay)^2)
400  IF L2-L1=0 THEN GOTO 430
410  Theta=ATN((By-Ay)/(L2-L1))
420  GOTO 440
430  Theta=90
440  PRINT L1,Ay,L2,By,Ab,Theta
450  PRINT #1;L1,Ay,L2,By
451  IF L2<200 THEN L2=0
452  IF L2>200 THEN L2=L1-200
460  L1=L1+10
470  NEXT I
480  DISP "COMPLETE"
490  ASSIGN #1 TO *
500  STOP
510  END
```

Figure 19

Program to Determine Velocity Vectors

TRACES 1-2-3

X	Y	VELOCITY	THETA
30.000	2198.592	.956	89.846
60.000	2192.351	.957	88.925
90.000	2186.284	.958	87.852
120.000	2180.235	.957	87.087
150.000	2174.050	.956	86.165
180.000	2167.574	.953	85.235
210.000	2160.653	.949	84.450
240.000	2153.131	.943	83.492
270.000	2144.855	.935	82.350
300.000	2135.669	.924	81.172
330.000	2125.420	.910	79.778
360.000	2113.952	.894	78.312
390.000	2101.110	.873	76.573
420.000	2086.741	.848	74.508
450.000	2070.689	.821	72.247
480.000	2052.800	.790	69.733
510.000	2032.920	.756	66.893
540.000	2010.892	.720	63.631
570.000	1986.564	.684	60.124
600.000	1959.780	.648	56.327
630.000	1930.386	.613	52.204
660.000	1898.227	.580	47.729
690.000	1863.148	.552	42.903
720.000	1824.995	.527	38.309
750.000	1783.613	.504	34.214
780.000	1738.848	.484	30.261
810.000	1690.544	.466	26.620
840.000	1638.548	.450	24.287
870.000	1582.704	.435	22.807

Table I. Numerical results of velocity vector computations for laser traces 1-2, 2-3.

TRACES 2-3-4			
X	Y	VELOCITY	THETA
30.000	2571.074	.681	90.000
60.000	2566.494	.695	89.138
90.000	2561.820	.705	88.521
120.000	2556.927	.712	87.917
150.000	2551.688	.715	87.318
180.000	2545.976	.715	86.714
210.000	2539.665	.713	86.099
240.000	2532.627	.707	85.467
270.000	2524.738	.699	84.598
300.000	2515.868	.688	83.690
330.000	2505.894	.674	82.508
360.000	2494.687	.657	81.250
390.000	2482.120	.637	79.899
420.000	2468.069	.615	77.921
450.000	2452.405	.589	76.020
480.000	2435.003	.563	73.322
510.000	2415.735	.536	70.601
540.000	2394.475	.508	67.515
570.000	2371.097	.482	63.989
600.000	2345.473	.458	60.376
630.000	2317.478	.437	56.734
660.000	2286.985	.418	53.686
690.000	2253.867	.403	50.919
720.000	2217.997	.390	48.587
750.000	2179.249	.381	46.864
780.000	2137.497	.375	46.646
810.000	2092.613	.372	47.452
840.000	2044.471	.374	48.630
870.000	1992.945	.383	50.953

Table II. Numerical results of velocity vector computations for laser traces 2-3, 3-4.

TRACES 1-3-2-4

X	Y	VELOCITY	THETA
30.000	2344.307	.878	89.831
60.000	2340.773	.883	88.997
90.000	2336.921	.887	88.172
120.000	2332.633	.888	87.517
150.000	2327.790	.888	86.693
180.000	2322.276	.885	86.030
210.000	2315.971	.881	85.187
240.000	2308.760	.875	84.327
270.000	2300.523	.866	83.442
300.000	2291.142	.855	82.349
330.000	2280.500	.841	81.209
360.000	2268.480	.823	79.821
390.000	2254.962	.803	78.150
420.000	2239.830	.780	76.353
450.000	2222.966	.754	74.179
480.000	2204.250	.724	71.779
510.000	2183.567	.693	68.838
540.000	2160.798	.662	65.778
570.000	2135.824	.632	62.588
600.000	2108.529	.602	59.266
630.000	2078.794	.574	55.825
660.000	2046.502	.549	52.294
690.000	2011.535	.526	49.203
720.000	1973.774	.507	46.250
750.000	1933.102	.490	44.116
780.000	1889.401	.475	42.459
810.000	1842.554	.463	41.429
840.000	1792.441	.456	41.182
870.000	1738.947	.451	42.590

Table III. Numerical results of velocity vector computations for laser traces 1-3, 2-4.

LIST OF REFERENCES

1. National Committee for Fluid Mechanics Films, Illustrated Experiments in Fluid Mechanics, MIT Press, 1972, 35, 66, 67, 146-147, 89-95.

2. Small, J. G., "The $30 Dye Laser", Physics of Quantum Electronics, 4, 343-353.

3. Popovich, A. T. and Hummel, R. L., "A New Method for Nondisturbing Turbulent Flow Measurements very Close to a Wall", Chemical Engineering Science, 22, 1967, 21-25.

4. Hardwick, R. and Maser, H. S., "Photochromatic Behavior of 2-(2', 4'-Dinitrobenzyl)-Pyridine", Transactions of Faraday Society, 56, 1960, 44-50.

5. Masher, H. S., "Flash Photolysis Studies of C- and Y-(2, 4-Dinitrobenzyl)-Pyridine", Journal of Chemical Physics, 37, no. 4, 1962, 904-909.

6. Popovich, A. T. and Hummel, R. L., "Experimental Study of the Viscous Sublayer in Turbulent Pipe Flow", AIChE Journal, Sept 1967, 854-860.

7. Berman, E., Fox, R. E., and Thompson, F. D., "Photochromatic Spiropyrans. I. The Effect of Substitutes on the Rate of Ring Closure", American Chemical Society Journal, 74, 1959, 5605-5608.

8. Poutanen, A. A. and Johnson, A. I., Canadian Journal of Chemical Engineering, 38, 1969, 93.

9. Humphrey, J.A.C., Canadian Journal of Chemical Engineering, 52, Feb 1974.

10. Devlin, J. C., M.S. Thesis D4598, Naval Postgraduate School, 1978.

11. Humphrey, J., Hummel, R. and Smith, J. W., "Experimental Study of the Internal Fluid Dynamics of Forming Drops", Canadian Journal of Chemical Engineering, 52, August 1972.

12. Culbreth, W., Johnson, G., and Marshall, E., "Heat Transfer and Hydrodynamics during Drop Formation and Release in a Liquid Heat Exchanger", AIChE Symposium Series, 1981.

13. Strong, C. L., "The Amateur Scientist", Scientific American, June 1974.

14. Holman, J. P., Experimental Methods for Engineers, 3rd ed., McGraw-Hill, 1978, 44-51.

INITIAL DISTRIBUTION LIST

		No. Copies
1.	Defense Technical Information Center Cameron Station Alexandria, Virginia 22314	2
2.	Library, Code 0142 Naval Postgraduate School Monterey, California 93940	2
3.	Chairman, Code 69Mx Department of Mechanical Engineering Naval Postgraduate School Monterey, California 93940	1
4.	Professor William G. Culbreth, Code 69Cb Department of Mechanical Engineering Naval Postgraduate School Monterey, California 93940	5
5.	LT August F. Pellin III, USN 575 N. Four Mile Run Road Youngstown, Ohio 44515	3